Flow Visualisation of Shock Wave Unsteadiness Applied in Shadow Graph System by using Space and Time Correlations

N. Vairamuthu
Assistant Professor
Dept of AERO- PITS

S. Priyadharshini
Dept of AERO- PITS

K. Pradeepa
Dept of AERO- PITS

Abstract:- **This paper fully describes the unsteady flow of normal flow in the shadowgraph system. In a supersonic wind tunnel provides a mach number more than 1.5 to the test section entrance area. And this data are used to analyzed to find out the normal shock wave unsteadiness, variations in frequency by time and space correlations, it gives coherence in time and perturbation in a different flow region. It includes the complexity of separate shockwave boundary layer and frequency. The auto correlation includes is to find out the two point function magnitude quantify. It time scale periodic events and then the coherence flow of perturbation in a region. It also prescribes the time lag and flow coherence by a spatial variation, is applied in single location associated in the normal shock wave.**

Keywords: Shock wave, Supersonic flow, Time correlation, Spatial correlation, Autocorrelation, Two-point correlation, Frequency spectra, Magnitude squared coherence, Time lag, flow analysis, Unsteady flow analysis.

1 INTRODUCTION

Shock wave boundary layer interactions occur in many aerospace applications. Some examples include ramjet isolator ducts, turbine blade tip gaps, and transonic wings. However, low frequency unsteadiness associated with shock wave boundary layer interactions is not well understood and continues to be a debated topic. This is because different studies concluded different and contradicting results. Some results indicated that shock wave unsteadiness originates from the turbulence in the upstream boundary layer. Other results indicated that a separation region formed as part of the shock wave boundary layer interaction generates the unsteadiness. Still other studies showed that both the upstream and downstream sources are responsible for shock wave unsteadiness. Clemens and Narayana swamy [1] summarized some of the possibilities. Many methods and analysis approaches were used to collect and analyze associated data. For example, power spectral densities and cross correlations were often used, especially for wall pressure signal data. Many of these investigations also employed. Schlieren and shadowgraph imaging to determine unsteady and spatially-varying shock wave structure. Erengil and Dolling [2], Handa et al. [3], Dupont et al. [4], and Bruce and Babinsky [5], among others, measured static pressure variations with time. Spatial pressure variations were then associated with shock wave position and motion. Power spectral densities were computed from time sequence pressure data at specific locations to determine the frequencies of the unsteadiness at various locations in the flow field. Bruce and Babinsky [5] also used schlieren imaging to determine the streamwise location of the shock wave. Gamba [6] used shock wave position with respect to time, in addition to the single location pressure measurements, to determine unsteadiness characteristics. Cross-spectrum and time lag were computed for pressure fluctuations and shock wave positions, such that pressure fluctuations were given relative to the position of the upstream most shock wave. Ganapathi subramani et al. [7] and Humble et al. [8] computed cross correlations between turbulent structures in the upstream boundary layer and the shock wave from particle image velocimetry data. They detected significant coherence between the turbulent structures in the upstream boundary layer and the shock wave motion. Other recent investigations which considered different methods of shock wave data analysis were described by Ganapathisubramani and Clemens [9], Wu and Martin [10], Piponniau et al. [11], Pirozzoli et al. [12], Touber and Sandham [13], and Grilli et al. [14]. Settles [15] also provided useful information in regard to schlieren and shadowgraph visualization techniques. The present investigation differs from many previous studies by providing greater detail of the analysis techniques used, and by using digitized shadowgraph data to visualize shock wave structure. Considered are unsteady flow and structural characteristics of a normal shock wave, a lambda foot, and a separated turbulent boundary layer within a unique research test section. The supersonic wind tunnel facility, containing this test section, provides a Mach

number of approximately 1.54 at the test section entrance. The digitized shadowgraph flow visualization data are analyzed to provide grayscale spectral
energy variations with frequency, as well as time and space correlations, which give coherence and time lag properties associated with perturbations associated with different flow regions. As such, the current investigation is aimed at improved analysis techniques for shock-wave-boundary-layer-interactions, for better physical understanding of these flows, and for development of improved techniques for control and management of flow unsteadiness associated with particular shock wave arrangements.

2 EXPERIMENTAL APPARATUS AND PROCEDURES

2.1 SUPERSONIC WIND TUNNEL

The supersonic wind tunnel (which is also referred to as the SS/TS/WT or Super Sonic/Trans Sonic/Wind Tunnel) is a blow down type facility, which is located within the low-pressure piping system used in these experiments (which is a portion of the overall piping system) consists of an air compressor, a vertical air supply tank, a series of pressure relief valves manual gate valve, a pneumatic flow control valve, a pressure regulating gate valve, and an air diverter plenum with 12 cubic meter volume. This plenum is then followed by the test section segment, an exhaust plenum with a volume of 2 cubic meters, and an exhaust piping system. The volume of the vertical air supply tank is 14 cubic meters. The tank pressure rating is 2.1 MPa. As the facility is prepared for testing, one of two compressors (either a Quincy QR 350, model BM350HPDT compressor with a ZEKS 75NDQCA100 air dryer, or a Bauer BP26-E3 compressor) fills the vertical supply tank with dried air. After the tank is pressurized to the appropriate supply pressure, the compressor is shut down and the small Ham-Let H700SSL3/4TLD manual ball valve between the compressorand the supply tank is closed. As a blow down test is conducted, air flows through a 152.6mm diameter pipe, which is located downstream of the vertical supply tank. A NEWCO N36726 manual gate valve, a Truline 330AITFM-CH-SQ pneumatic flow control ball valve, and a Fisher Valves Type 667-EWT-DVC6200 pressure regulating valve are located along this pipe. The manual gate valve is open fully during testing. The pneumatic flow control ball valve is also fully open during testing. The pressure regulating valve is controlled by a Fisher FIELDVUE DVC6200 Digital Valve Controller. The digital valve controller is set to maintain a constant downstream pressure of 413.7 kPa as an individual blow down test is underway. Downstream of the pressure regulating valve, the air flows into the air diverter plenum. Six Kunkle 913BFEM03 pressure relief valves provide means to vent over-pressurized air, both before and after the manual gate valve. Flow static pressure is measured before and after each control valve within the piping system, using both Ashcroft analog pressure gauges and Honeywell FPA 060-C860–15 digital pressure transducers.
Three independent wind tunnel segments are connected to the downstream parts ofthe air diverter plenum. Three additional Kunkle 913BFEM03 pressure relief valves and a burst disk are additionally mounted on the air diverter plenum for pressure relief in the unlikely event of over-pressurization. A spectacle blind valve or a circular sliding
gate valve is located at the inlet to each of the wind tunnel segments. To conduct a test with one such segment, the associated inlet valve is open, whereas valves at the inlets of the other segments are closed. The research test section, which is employed for the present study, is used as one of the wind tunnel segments. This segment includes a spectacle blind valve, which is followed by a straight inlet duct, a converging/diverging supersonic nozzle, the test section, an exhaust diffuser and plenum, and an exhaust piping system with three independent noise baffles. Each noise baffle bolts to the associated 203mm exhaust duct by means of a flange, and is approximately 1m in length, with an inner diameter of 203 mm. The converging diverging nozzle accelerates the flow to supersonic velocities. The flow then enters the test section. The test section is constructed with a flat bottom wall a diverging top wall, and two side walls. The test section contains a shock wave holding plate and a choking flap. The angle of the choking flap, as well as the normal and stream wise positions of the shock wave holding plates, are all adjustable
The exhaust plenum includes four air exhaust duct vents. Two 203mm diameter exhaust ducts vent the air outside of the laboratory through 7.6m of straight 203mm diameter pipe. A 38 mm diameter vent vents to the air inside of the laboratory. These three vents are always open. A Kunkle 913BFEM03 pressure relief valve and a burst disk are additionally mounted on the plenum for pressure relief in the unlikely event of over-pressurization. A 102mm diameter vent is also installed on the exhaust plenum. This particular vent includes a custom made spectacle blind valve which is adjustable. For the present tests, the 102mm diameter exhaust passage is half-open.

2.2 SHADOWGRAPH OPTICAL FLOW VISUALIZATION SYSTEM

During wind tunnel tests, an Edmond Optics Corporation shadowgraph system records time-varying, shock wave flow features within the test section. The system consists of a white light source and two 152.4mm diameter focusing mirrors. The light source produces a beam of light that is reflected off the first mirror. The beam is then columnated as it passes through the test section. Because each viewed image is generally invariant in the span wise direction, the mirrors are aligned such that the light beam is parallel to the span wise direction and orthogonal to the side walls. This alignment provides the images with the greatest contrast and visualization of density-varying flow features. The second mirror additionally focuses the resulting shadowgraph image into the NIKKOR 200mm lens, which is connected to a Phantom v711 camera. This high speed camera captures a time sequence of digitized flow visualization images during each wind tunnel test. Phantom Camera Control Application 2.7 software then processes the images which are captured by the camera. The Phantom v711 Camera has a 20 μm resolution at all sampling rates, and can acquire a sequence of images at rates as high as 1400 kHz. Figure 1 shows an example instantaneous

shadowgraph image, obtained with this apparatus, as part of the present investigation.

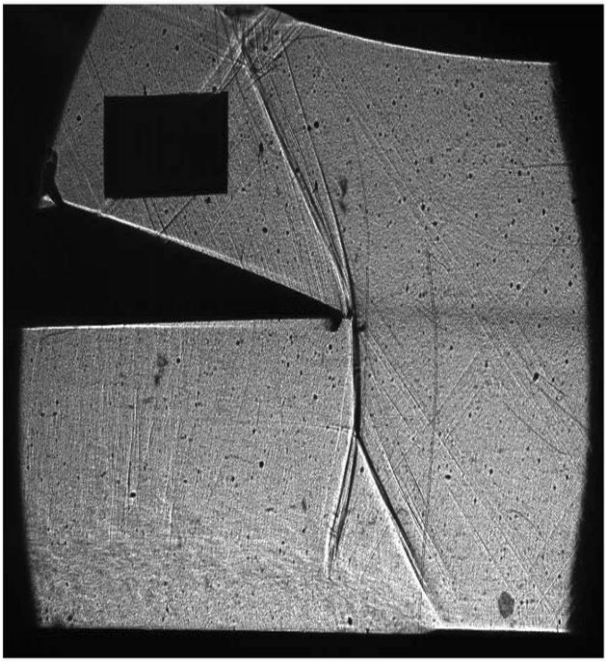

FIG: SHADOWGRAPH FLOW VISUALIZATION IMAGE FOR DATA ILLUSTRATING THE PRESENCE OF A NORMAL SHOCK WAVE, LAMBDA FOOT, AND SEPARATED TURBULENT BOUNDARY LAYER WITHIN THE LOWER FLOW PASSAGE, AND AN OBLIQUE SHOCK WAVE SYSTEM WITHIN THE UPPER FLOW PASSAGE.

2.3 PRESSURE MEASUREMENTS

Surface static pressures are measured within the test section, the exhaust plenum, and downstream of the pressure regulating valve. The static pressure tap used for this purpose within the test section is located along the centerline of the bottom wall, upstream of the shock wave. Each pressure is measured using a Honeywell FPA 060-C54985172080 digital pressure transducer. Each transducer is connected to a National Instruments Voltage Input Module, NI 9209, mounted within a NI Compact-DAQ USB Chassis, NI cDAQ-9174. These devices together convert the analog voltage signal from the transducers into a digital signal which is readable using Lab VIEW 2015 Full Development System version 15.0f2 software.

2.4 EXPERIMENTAL TESTING PROCEDURE

Wind tunnel tests typically last approximately eight seconds from the time the pressure regulating valve is opened to the time it begins to close. For the majority of tests, data are captured from a time before the pressure regulating valve is opened, until after the flow stops. Flow conditions are typically established and maintained for about five seconds during each test. Only this portion of the wind tunnel test is considered during the subsequent analysis. The shadowgraph images captured during start-up and shut-down, prior and after flow is established, are generally discarded.

2.5 DATA ANALYSIS PROCEDURES

The digitized time sequence of flow visualization images are processed to compute frequency spectra, and different correlations using National Instruments' Lab VIEW 2015 Full Development System version 15.0f2 software, and Math works' MATLAB versions R2014b through R2018a software.

2.5.1 ANALYSIS OF FLOW VISUALIZATION TIME SEQUENCE DATA AND DETERMINATION OF FREQUENCY SPECTRA

Frequency spectra are computed in six steps: extract data for a particular pixel location, filter the data, transform and normalize the data into the frequency domain, smooth the frequency domain results, remove the white noise, and ensemble average the data associated with multiple pixel locations.

2.5.2 EXTRACT PIXEL DATA

For a selected collection of images, a MATLAB program extracts the time sequence of grayscale values at any specified pixel. During a wind tunnel test, flow conditions are established and maintained for a time interval. Only this portion of the wind tunnel test is considered during the analysis. The MATLAB code used to extract grayscale value data from specific pixels in the images has three necessary inputs. The user indicates which pixel to analyze, the file path to the folder of bitmap images during established flow conditions, and the output file name. MATLAB's "In read" function determines the grayscale value of the specified pixel for each image in the folder. The output is a time sequenced array of grayscale values. MATLAB's "xlswrite" function saves the associated array in a Microsoft Excel spreadsheet.

2.5.3 FILTER THE TIME SEQUENCE

The time sequence of grayscale values must be read into Lab VIEW software in order to be filtered. The file path to the saved text file is specified within a subroutine in Lab-VIEW called the "Read from Measurements File" Express VI. The subroutine imports the time sequence of grayscale values into Lab VIEW from the tab delimited text file. Once in Lab VIEW, the data is converted from the dynamic data type to an array of double precision floating point values. A low-pass Butterworth filter is used to filter the time sequence data.

A Butterworth filter is used, as opposed to another type of filter, because of its relatively uniform transfer function scaling over the frequencies of interest. The transfer function is the ratio of the filtered value to the unfiltered value as a function of frequency. Uniform scaling over the transfer function is important because it does not add extraneous frequency content to the data. This ensures that any peaks in the frequency domain data are from real events, not distortion from the filter.

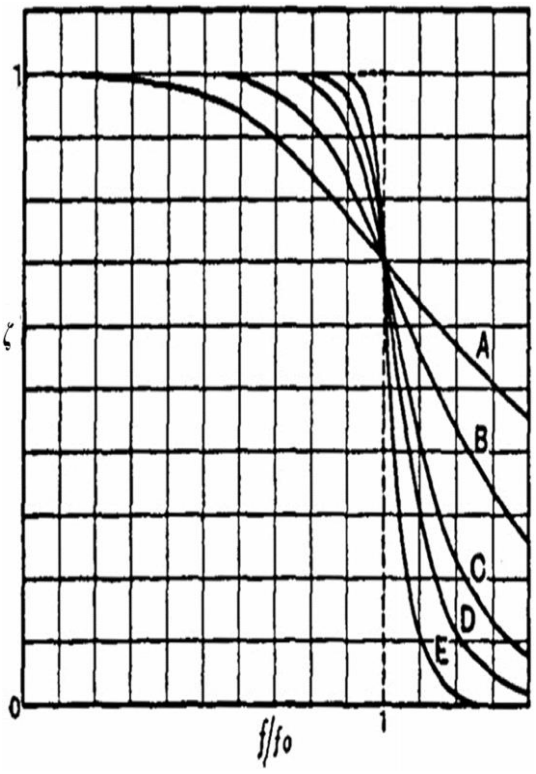

FIG. THE TRANSFORM FUNCTION OF A LOW PASS BUTTERWORTH FILTER.

The time sequence array of grayscale values is filtered with a fifth-order, low-pass Butterworth filter, using a cut-off frequency of 1 Hz less than the Nyquist folding frequency. The filtering is done with Lab VIEW's "Butterworth Filter" VI subroutine. The
data, the cut-off frequency, the sampling rate, the type of filter (low pass, for example), and the order of the filter are inputs to this subroutine. This output is the filtered data as an array of double precision floating point values. After being filtered, the data are converted to a dynamic data data type. The resulting filtered data are saved to a tab delimited spreadsheet.

2.5.4 REMOVE WHITE NOISE

The white noise is associated with the background electronic noise within the time series signal. The next step in the analysis is to subtract the white noise from the frequency domain data. The average value that replaces the grayscale spectral energy distribution data corresponding to frequencies greater than 95% of the Nyquist folding frequency during the smoothing process is considered the white noise energy content level. The same value of the white noise energy content level is subtracted from every
spectral data point at each frequency within the smoothed frequency array. Note that each image pixel is associated with a unique frequency transform and therefore a unique white noise energy content level. Removing the white noise gives greater frequency.

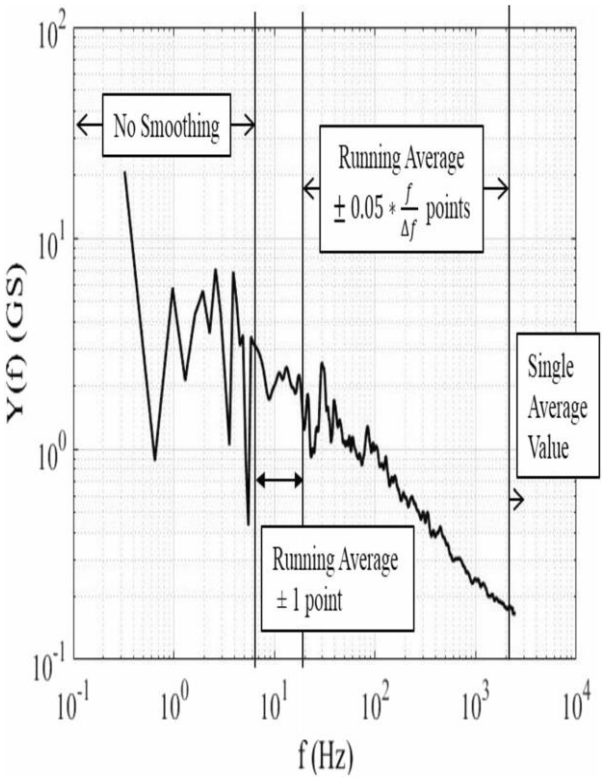

FIG: GRAYSCALE SPECTRAL ENERGY DISTRIBUTION AFTER SMOOTHING.

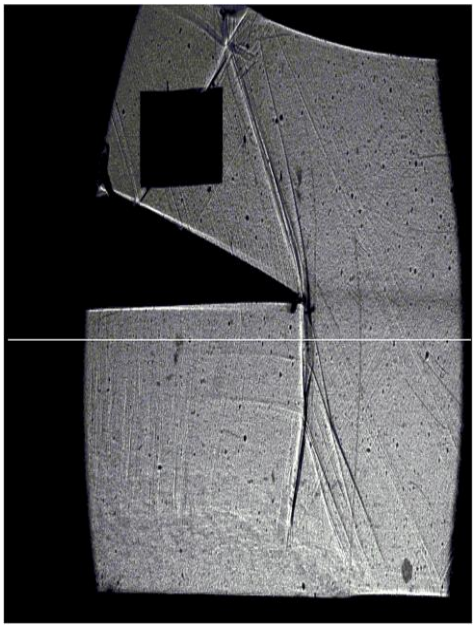

FIG: SHADOWGRAPH FLOW VISUALIZATION IMAGE, WHERE HORIZONTAL WHITE LINE INDICATES PIXEL LOCATIONS WHERE THE GRAYSCALE DATA ARE ANALYZED

3 EXPERIMENTAL RESULTS AND DISCUSSION

3.1 TEST SECTION FLOW CHARACTERISTICS

The main flow Mach number at the test section inlet is approximately 1.54. This value is determined from the inlet nozzle design, and is confirmed by measurements of local static pressure and local stagnation pressure. The associated test section mass flow rate is approximately 12.5 kg/s. Local boundary layer thickness is estimated to be approximately 10.5mm on the top and bottom walls of the test section at a streamwise location which is just upstream of the leading edge of the shock wave holding plate.When steady flow conditions are established within the test section, the absolute pressure downstream of the pressure regulator is approximately 380 kPa. Static absolute pressure upstream of the shock wave in the test section is approximately 97 to 98 kPa, and the absolute pressure within the exhaust plenum is 130 kPa..

3.2 OVERALL FLOW STRUCTURE

This figure presents an instantaneous shadowgraph flow visualization image for the 05 experimental result, illustrating the presence of a normal shock wave, a lambda foot, and a separated turbulent boundary layer located near the entrance of the lower flow passage, and an oblique shock wave system within the upper flow passage. Flow within this image is from right to left, with the shock wave holding plate evident within the left-hand side of the image. As such, the present experimental arrangement and resulting flow structure are similar. Flow visualization data are captured at an acquisition rate of 10.0 kHz during the test on 05 April 2018. A total of 21,619 images are collected, as steady flow conditions are maintained during this test. The frequency resolution is 0.4625 Hz. Each image size is 1024 × 512 pixels. To achieve the instantaneous result presented in Fig flow at the test section inlet must be uniform and steady, with relatively low free stream turbulence intensity, and no significant flow disturbances or non-uniformities. Note that a few oblique lines are evident within Fig on the right-hand side of the image, which are located just downstream of the test section inlet. These lines are due to the presence which are due to imperfections on the outside surfaces of the side walls of the wind tunnel. These spots have no effect on the flow.

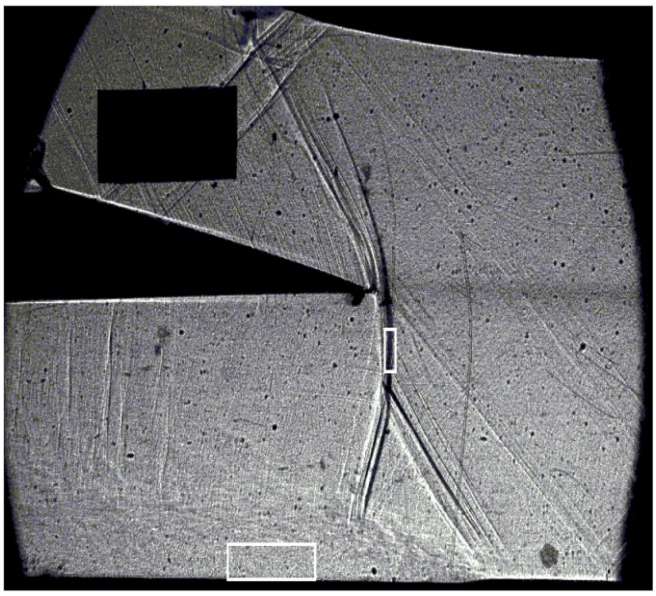

FIG: SHADOWGRAPH FLOW VISUALIZATION IMAGE, WHERE RECTANGLES MARK PIXEL LOCATIONS IN THE DOWNSTREAM BOUNDARY LAYER AND NEAR THE NORMAL SHOCK WAVE, WHERE TIME-VARYING DATA ARE ANALYZED TO OBTAIN THE RESULTS.

3.3 SHOCK WAVE STREAM WISE POSITION GRAYSCALE SPECTRAL ENERGY RESULT

A Lagrangian approach is used to determine the spectral energy distribution associated with the stream wise location of the normal shock wave, as discussed earlier. At a vertical location marked by the white line in the shock wave position changes approximately 6mm in either direction, relative to its average position, due to shock wave unsteadiness. Note that the shock wave is positioned slightly downstream of its average position in this shadowgraph image. The resulting grayscale energy spectrum is shown .This is compared with the ensemble-averaged grayscale spectral energy distribution (determined for five closely-located pixel locations) near the shock wave, shown The grayscale spectral energy distributions at five pixel locations are ensemble-averaged to generate these results. The region in which these pixels are located is denoted by a white rectangle. Note that the show peaks at similar frequencies. For example, both data sets show spectral peaks at approximately 40Hz and between 2Hz and 9Hz. It also show that the spectral energy decreases significantly for frequencies greater than 200 Hz.

3.4 AUTO-CORRELATION FUNCTION RESULT

The auto-correlation is calculated for data associated with a specific pixel location. For the present result, a pixel location associated with the shock wave is considered. The auto-correlation of this time sequence data .Significant positive values are evident at 0.0 s, 1.4 s, and 0.75 s. Values for approximately 0.75 s indicate that the associated correlation is relatively weaker, since the auto-correlation magnitude barely exceeds the 95% confidence interval. Negative values of the auto-correlation indicate that the data are strongly dissimilar at time lags of 0.4 s and 0.9 s. Overall, the data show that gray scale time sequence data

are roughly cyclical, with the most pronounced oscillation time period equal to approximately 1.4 s.

3.5 CORRELATION FUNCTION VARIATIONS BETWEEN SHOCK WAVE AND DOWNSTREAM BOUNDARY LAYER REGIONS

Magnitude squared coherence and time lag variations are determined between data associated with the shock wave and the downstream boundary layer. The regions containing the locations of the pixels that are analyzed are shown by white rectangle. It shows the magnitude squared coherence of the time sequence grayscale signals in these two regions with respect to frequency. Associated data values evidence significant coherence between the shock wave, and downstream boundary layer regions, at frequencies of approximately 6 Hz, 20 Hz, 40 Hz, and 100 Hz, which correspond to respective Strouhal numbers of 0.00079, 0.00263, 0.00526, and 0.0132. Note that the Hanning windowing creates some fluctuations in the results at high frequencies,

which are not representative of true coherence. Time lag values from grayscale flow visualization results are shown in Fig. 18, also for perturbations between the downstream boundary layer and the shock wave. Perturbations of approximately 20 Hz, 30 Hz, and 70 to 100 Hz occur in the downstream boundary layer prior to the same frequency events in the shock wave. This is determined because values of time lag are positive for these different frequencies. At 100 Hz, perturbations in the downstream boundary layer occur approximately 1 ms before they do in the shock wave. However, for events at frequencies of approximately 5 Hz, 10 Hz, 40 Hz, and 60 Hz, time lag values are negative, indicating that the perturbations in the shock wave occur prior to

the ones in the downstream boundary layer. Note that all of these time lags are approximately an order of magnitude longer than time lags associated with the estimated advection speed of the fluid.

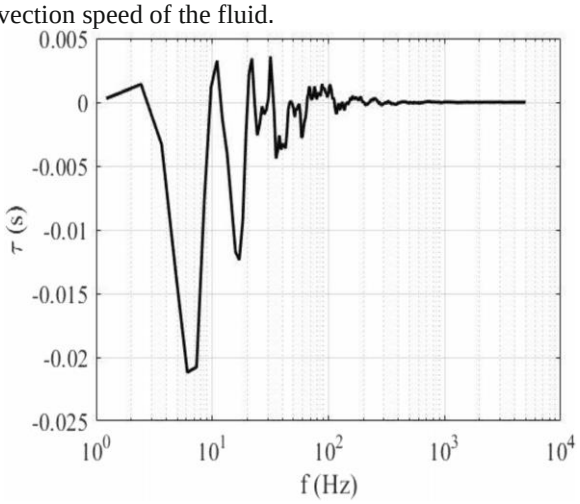

FIG: TIME LAG MAGNITUDE VARIATION WITH FREQUENCY OF DATA ASSOCIATED WITH LOCATIONS NEAR THE SHOCK WAVE AND IN THE DOWNSTREAM BOUNDARY LAYER,. NOTE THAT POSITIVE TIME LAG VALUES INDICATE THE SIGNAL IN THE BOUNDARY LAYER (FOR A PARTICULAR FREQUENCY) OCCURS PRIOR TO THE SIGNAL (AT THE SAME FREQUENCY) WHICH IS ASSOCIATED WITH THE NORMAL SHOCK WAVE.

3.6 CORRELATION FUNCTION AND TIME LAG RESULTS TO ILLUSTRATE SPATIAL VARIATIONS

The magnitude squared coherence and time lag at certain frequencies are determined for one location, relative to a range of other spatial locations. The locations are represented by the vertical white line within the flow visualization image . Note that coordinate scale locations along this line are included. The magnitude squared coherence and time lag are calculated between these locations and a location on the shock wave, which is indicated by a white dot The origin is chosen to be the

location of the pixel on the shock wave. The other pixel locations are measured relative to that location. Magnitude squared coherence values and magnitudes of time lag between the same shock wave pixel location and the pixels along the vertical line on the shock wave are a frequency of 40 Hz. This figure shows a magnitude squared coherence of 1.0, and a time lag of 0 s, at the location where y1 is the same as y2. This is because any signal is completely coherent with itself. For a frequency of 40 Hz, a peak in the coherence is evident approximately 12.7mm beneath the location of y2. Note that this location approximately corresponds to the intersection point between the normal shock wave and the two oblique shock wave legs of the lambda foot. Associated time lag results in show that little coherence is generally present for locations where time lag values are notable. The most significant time lag value is negative and is evident at a location about 7mm below the single shock wave pixel location. This means that events for the single shock wave position y2 occur prior to events associated with the location 7mm below, which is associated with y1. With larger values of coordinate z, time lag values are then either near zero or show large amounts of data scatter.

4. CONCLUSIONS

Within the present study, investigated are unsteady flow characteristics of a normal shock wave, a lambda foot, and a separated turbulent boundary layer within a unique research test section. The supersonic wind tunnel facility, containing this test section, provides a Mach number of approximately 1.54 at the test section entrance. A shadowgraph optical system is employed to visualize shock wave structure within the test section.

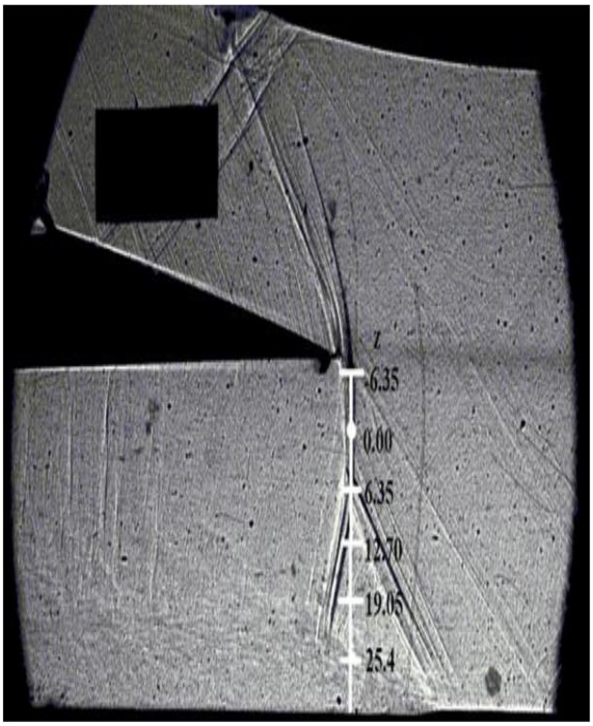

FIG: SHADOWGRAPH FLOW VISUALIZATION IMAGE, WHERE WHITE DOT AND WHITE LINE SHOW LOCATIONS

A Lagrangian approach is used to determine the spectral energy distribution associated with the stream wise location of the normal shock wave, The resulting grayscale energy spectrum is compared with an ensemble-averaged grayscale spectral energy distribution (determined for five closely-located pixel locations), which shows that both results evidence peaks at similar frequencies at approximately 40 Hz and between 2 Hz and 9 Hz. Auto-correlation function results show that the time sequence of grayscale values, for particular shock wave locations, is approximately cyclical, with a period of approximately 1.4 s.Two-point correlation functions, as they vary with frequency, indicate that perturbations at a frequency of 100 Hz (Str = 0.0130) originate downstream of the shock wave and propagate upstream. Magnitudes of time lag between one stationary shock wave pixel location, and
the pixels along the vertical line along and near to the shock wave, show that the most significant time lag value is negative and is evident at a location about 7mm below the single shock wave pixel location. This means that events for the single shock wave position occurprior to events associated with the location 7mm below that position.

REFERENCES

[1] Clemens NT, Narayanaswamy V (2014) Low-frequency unsteadiness of shock wave turbulent boundary layer interactions. Ann Rev Fluid Mech 46:469–492
[2] Erengil ME, Dolling DS (1991) Correlation of separation shock motion with pressure fluctuations in the incoming boundary layer. AIAA J 29:1868–1877
[3] Handa T, Masudo M, Matsuo K (2003) Mechanism of shock wave oscillation in transonic diffusers. AIAA J 41:64–70
[4] Dupont P, Haddad C, Ardissone JP (2005) Space and time organization in a shock wave/turbulent boundary layer interaction. Aerosp Sci Technol 9:561–572
[5] Bruce PJK, Babinsky H (2008) Unsteady shock wave dynamics. J Fluid Mech 603:463–473
[6] Gamba M (2016) Roles of flows in a corner on the orderly response of a Mach 2 shock train. 10th Annual SWBLI TIM, Dayton, Ohio, USA
[7] Ganapathisubramani B, Clemens NT (2009) Low frequency dynamics of shock induced separation in a compression ramp interaction. J Fluid Mech 636:397–436
[8] Analysis of shock wave unsteadiness using space and time correlations applied to shadowgraph flow visualization data.